

Multi Voxel-Point Neurons Convolution (MVPConv) for Fast and Accurate 3D Deep Learning

Wei Zhou

Northwest University
mczhouwei12@gmail.com

Xin Cao

Northwest University
xin_cao@163.com

Xiaodan Zhang

Northwest University
xiaodanzhang@nwu.edu.cn

Xingxing Hao

Northwest University
ystar1991@126.com

Dekui Wang

Northwest University
dekui.wang@126.com

Ying He

Nanyang Technological University
yhe@ntu.edu.sg

Abstract

We present a new convolutional neural network, called *Multi Voxel-Point Neurons Convolution (MVPConv)*, for fast and accurate 3D deep learning. The previous works adopt either individual point-based features or local-neighboring voxel-based features to process 3D model, which limits the performance of models due to the inefficient computation. Moreover, most of the existing 3D deep learning frameworks aim at solving one specific task, and only a few of them can handle a variety of tasks. Integrating both the advantages of the voxel and point-based methods, the proposed MVPConv can effectively increase the neighboring collection between point-based features and also promote the independence among voxel-based features. Simply replacing the corresponding convolution module with MVPConv, we show that MVPConv can fit in different backbones to solve a wide range of 3D tasks. Extensive experiments on benchmark datasets such as ShapeNet Part, S3DIS and KITTI for various tasks show that MVPConv improves the accuracy of the backbone (PointNet) by up to **36%**, and achieves higher accuracy than the voxel-based model with up to **34×** speedup. In addition, MVPConv also outperforms the state-of-the-art point-based models with up to **8×** speedup. Notably, our MVPConv achieves better accuracy than the newest point-voxel-based model PVCNN (a model more efficient than PointNet) with lower latency.

1. Introduction

3D deep learning for point clouds has received much attention in both industry and academia thanks to its potential for a wide range of applications, such as autonomous driving and robots. The main technical challenges are due to the sparse and irregular nature of point clouds.

The existing 3D deep learning methods can be roughly divided into voxel- and point-based methods according to the representations of point clouds. The voxel-based methods convert the irregular and sparse point clouds into regular 3D grids so that the widely studied convolutional neural networks (CNN) can be applied directly [6, 33, 57]. Since their performance heavily depends on the voxelization resolution, the voxel-based methods often suffer from large information loss when the resolution is low, as multiple adjacent points are quantized into the same grid, which are indistinguishable. Conversely, a high resolution volume would preserve the fine-detailed information, but requires significant amount of GPU memory and computation time due to the cubic complexity of volumes. In contrast, the point-based methods can handle high-resolution models, since they process the raw points in a local and separate manner [14, 19, 28, 30, 47]. Taking advantage of the sparse representation of point clouds, the point-based methods consume much less GPU memory than the voxel-based methods. However, due to lack of regularity, they suffer from expensive random memory access and dynamic kernel computation during the point and its nearest neighbor searching [23].

Motivated by the merits and limitations of each type of methods, several researchers proposed mixed representations to overcome the challenges of high accuracy demand and limited computational resources available on GPUs recently [23, 5, 36, 55, 38, 35]. However, most of these point-voxel combined methods are only for solving a specific task with a point-voxel based framework. For example, PV-RCNN [35] and PV-RCNN++ [36] focus on 3D object detection, and Pvdeconv [5] targets 3D auto-encoding CAD construction, FusionNet [55] is for semantic segmentation. Tang *et al.* proposed a sparse point-voxel convolution for efficient 3D architecture searching [38]. To our knowledge, there is no general point-voxel based method for solving different kind of tasks.

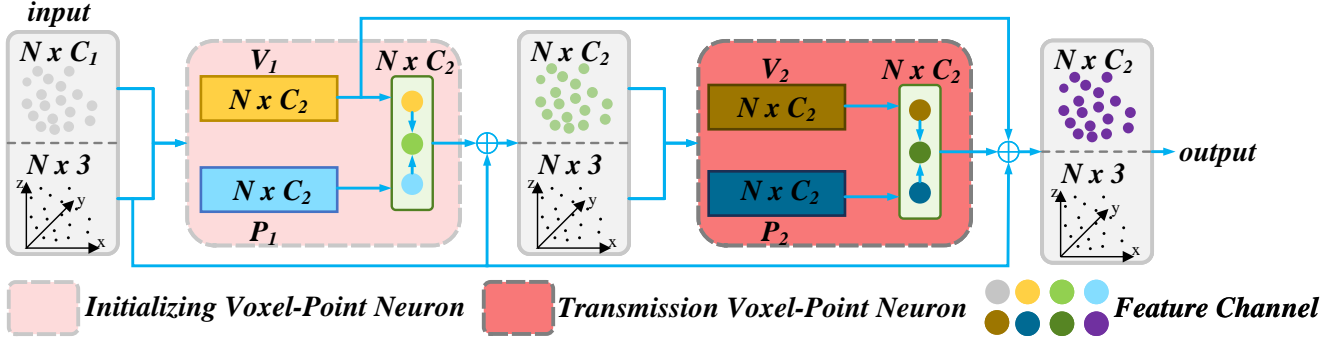


Figure 1. The proposed MVPCConv increases the neighboring collection between point-based features and the independence among voxel-based features via adopting both 3D CNN and MLPs on both point-based and voxel-based features.

To design effective deep neural networks for 3D analysis, one must take into consideration the performance, efficiency, as well as generality and flexibility for various tasks. In this paper, we propose Multi Voxel-Point Neurons Convolution (MVPCConv) which takes the advantages of both the voxel- and point-based methods, and can work with different backbones for a wide range of 3D tasks (see Figure 1). In the previous 3D CNN models, the point-based features are individual and the voxel-based features are based on local neighborhood. In contrast, our MVPCConv conducts 3D CNN and MLP on both points and voxels. As a result, it increases not only the neighboring collection for point-based features, but also the independence among voxel-based features. Extensive experiments show that MVPCNN outperforms the state-of-the-art 3D CNN models in terms of accuracy and efficiency.

2. Related Work

Voxel-based 3D learning. Inspired by the success of CNN on 2D images [43, 32, 31], researchers transfer point cloud representation to volumetric representation and attempt to adopt convolution over it [25, 6, 29, 17, 7]. As is known to all, the larger the voxel resolution is, the more detailed feature information is contained, and the calculation of 3D volumetric convolution increases exponentially. To slow down this problem, researchers adopt octree to construct efficient convolutional architectures to increase the efficiency of computation with high voxel resolution [39, 33, 39]. State-of-the-art researches have demonstrated that volumetric representation can also be applied in 3D shape classification [50, 46, 17], 3D point cloud segmentation [10, 26, 48] and 3D object detection [57]. Although the voxel-based methods have a great advantage in data structuring for 3D CNN, its computation efficiency is still greatly limited by the size of voxel resolution.

Point-based 3D learning. PointNet [28], the first deep neural network, takes advantage of spacial transform network (STN) and simple symmetric function (maxpooling)

to process 3D point clouds. Many follow-up researches improve PointNet by aggregating hierarchically to extract the local features [30, 14]. PointCNN [19], SpiderCNN [54] and Geo-CNN [15] dynamically generate local geometric structure to capture points' neighboring features. RSNet [11] adopts a lightweight local dependency module to efficiently model local structures of point clouds. 3D-GCN [20], DGCNN [47], Grid-GCN [53], SpecConv [44], SPGraph [16], GAC [45] adopt graph convolutional networks to conduct 3D point cloud learning, while RS-CNN [22], PCNN [3], SCN [51] and KCNet [34] make use of geometric relations for point cloud analysis. Furthermore, SPLATNet [37] uses sparse bilateral convolutional layers to build the network, and SO-Net [18] proposes permutation invariant architectures for learning with unordered point clouds. SSNet [42] combines Morton-order curve and point-wise to conduct self-supervised learning. SPNet [21] uses a self-prediction for 3D instance and semantic segmentation of point clouds. As pointed out in [23], random memory access and dynamic kernel computation are the performance bottleneck of point-based methods.

Point-voxel-based 3D learning. Point-voxel-based methods combine the voxel- and point-based approaches. Aiming at 3D object detection, PV-RCNN [35] attracts the multi-scaled 3D voxel CNN features by PointNet++ [30], then the voxel- and point-based features are aggregated to a small set of representative points. Based on PV-RCNN, PV-RCNN++ [36] has improved the computation efficiency of point-based parts. Like PV-RCNN and PV-RCNN++ applied in 3D object detection, other point-voxel-based 3D learning methods [5, 55, 38] are specialized in 3D construction, 3D semantic segmentation or 3D structuring. PVCNN [23] adopts interpolation to obtain the voxel-based CNN features, and then aggregates the point-based features and the interpolated voxel-based features as output. Comparing with the existing point-voxel-based methods [23, 5, 36, 55, 38, 35], our method can deal with different kind of 3D tasks by applying MVPCConv in various backbones. Moreover, we use

shared MLPs to process the voxel-based features and adopt 3D CNN on the point-based features, thus improving the performances of different 3D deep learning tasks.

3. Multi Voxel-Point Neurons Convolution

State-of-the-art 3D deep learning methods are based on either voxel-based CNN methods or point-based network. Generally speaking, 3D voxel-based CNN method owns good data locality and regularity for low-resolution point neighbors (voxel grids), while the point-based approaches are independent for each point, so it could capture high-resolution information.

In this paper, we propose a new way to realize convolution for processing point cloud that named Multi Voxel-Point Neurons Convolution (MVPCConv) inspired by point-voxel-based methods and convolution operation. Instead of working on a specific 3D task like PV-RCNN [35], PV-RCNN++ [36], Pvdeconv [5] and FusionNet [55], our MVP-Conv could be applied in the backbone frameworks of different tasks (replacing the corresponding convolution in backbone with MVPCConv). Furthermore, the previous point-voxel-based methods (e.g. [35, 36, 23]) conduct the 3D CNN and MLP operations for the point and voxel separately, and finally gather the point-based and voxel-based features together. Unlike them, our MVPCConv performs both 3D CNN and MLP on both point and voxel.

As illustrated in Figure. 2, MVPCConv consists of two Voxel-Point neurons, the left neuron is initializing neuron, the right one is the transmission neuron, each neuron can be divided into the point-based and voxel-based modules. The point-based and voxel-based modules in these two neurons got big similarities: the point-based modules mainly use shared MLP to extract the independent features for each point, and it only consumes a small amount of memory for calculation even for high-resolution points; the voxel-based modules adopt 3D CNNs and interpolation to capture the neighboring points features, and it only cost a small GPU memory as the voxel resolution adopted in this paper is low.

3.1. Initializing Voxel-Point Neuron

The initializing Voxel-Point neuron is used to initialize the feature information from the input 3D data $X = \{\mathbf{x}_1, \dots, \mathbf{x}_n\} = \{(\mathbf{p}_1, \mathbf{f}_1), \dots, (\mathbf{p}_n, \mathbf{f}_n)\} \subseteq \mathbb{R}^{3+C_1}$, where \mathbf{p}_i is the 3D point coordinates $\mathbf{p}_i = (x_i, y_i, z_i)$, it may also contain further information, e.g. RGB color and normal; \mathbf{f}_i is the output feature of previous layer which includes C_1 channels.

3.1.1 Voxel-based Module of Initializing Neuron

3D CNN on voxel grid is a popular selection for state-of-the-art 3D deep learning researches. Due to its high regularity and efficient structuring with 3D CNN, we adopt the

voxel-based module to capture the initializing neighboring information for Voxel-Point neuron.

Point Transformation. Before we implement the Voxel-based module, we conduct point transformation to eliminate the influence from the translation and the scale variations of 3D points. Firstly, we calculate the mean point $\bar{\mathbf{p}}$ of the input 3D data, and translate each point with $\bar{\mathbf{p}}$ by $\mathbf{p}_i = \mathbf{p}_i - \bar{\mathbf{p}}$. Then we search the farthest point $\|\mathbf{p}\|_{max}$ as the radius, and transform the whole points into the unit sphere:

$$\hat{\mathbf{p}}_i = \frac{\mathbf{p}_i}{2 * \|\mathbf{p}\|_{max}} + 0.5 \quad (1)$$

where $\hat{\mathbf{p}}_i$ is the transformed point coordinates. During the experiments, we find that the transformation for feature is not necessary, as it reduces the accuracy results of our model. So, among this process, we just transform the point coordinates, and here we marked the transformed data as $\{\hat{\mathbf{p}}_i, \hat{\mathbf{f}}_i\}$.

3D Voxel CNN. After the point transformation, the coordinate range of each point is from 0 to 1, thus we enlarge the coordinate value from 0 to $r - 1$, where r is the resolution of voxel grid, and we marked the enlarged coordinates as $\hat{\mathbf{p}}_{ri}(\hat{x}_{ri}, \hat{y}_{ri}, \hat{z}_{ri})$. Then the points $\hat{\mathbf{p}}_{ri}$ and its corresponding features $\hat{\mathbf{f}}_i$ are voxelized into the voxels with low spatial resolution of $r \times r \times r$, and the features of voxels are the mean features of all inside points:

$$\mathbf{F}(u, v, w) = \frac{\sum_{i=1}^n \text{floor}(\hat{x}_{ri}, \hat{y}_{ri}, \hat{z}_{ri}) \cdot \hat{\mathbf{f}}_i}{n} \quad (2)$$

where $\mathbf{F}(u, v, w)$ is the features of voxels (u, v, w) , n is inside point number of (u, v, w) , and floor is the down rounding function. The influence of voxel resolution r will be discussed in Section 4.5. Next a series of $3 \times 3 \times 3$ 3D CNNs are adopted to aggregate the neighboring feature information of voxels. To capture the neighborhood information more accurately, we have increased the feature channels to C_2 during 3D CNN implementation.

Voxel Feature Interpolation. Then we interpolate the voxel features into the common domain of point cloud since we need to aggregate the information of voxel-based module and point-based module. The common operation for interpolation is the tri-linear interpolation and nearest-neighbor interpolation. Similar to the conduction in PVCNN, we adopt tri-linear interpolation to transform the voxel features into the point features $\mathbf{V}_1 = \{V_{11}, \dots, V_{1n}\} \subseteq \mathbb{R}^{C_2}$.

3.1.2 Point-based Module of Initializing Neuron

Although the voxel-based module aggregates the neighboring feature information for the input 3D data, its extracted information is in a coarse manner with low voxel resolution. In order to make up for this defect, we adopt point-based SharedMLP (1D convolution with kernel of 1) to make either efficient learning on each point for the input 3D data.

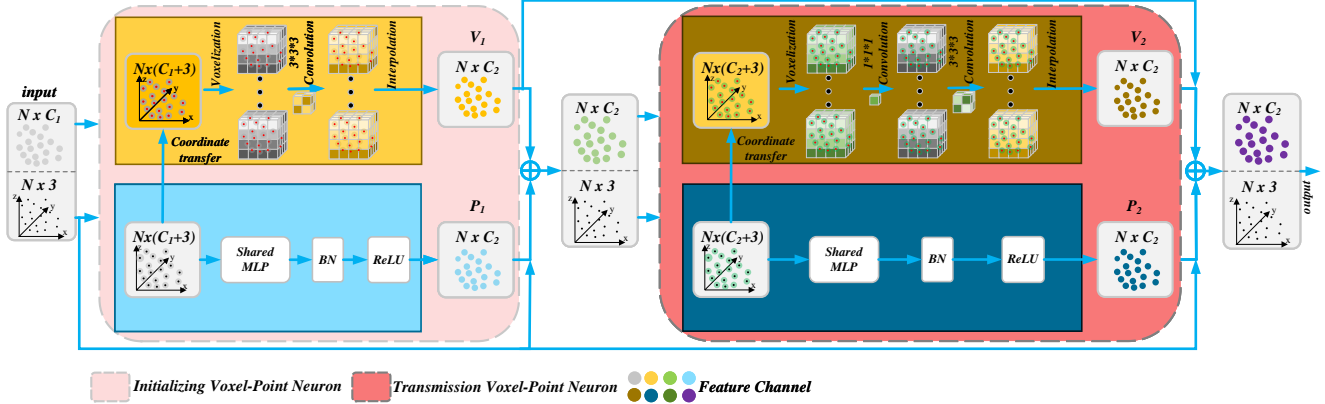


Figure 2. MVPCnn pipeline.

Table 1. Evaluation results of part segmentation on ShapeNet Part dataset.

Method	Reference	Type	Input Data	mIoU	GPU Mem.	latency
mIoU < 86.0						
Kd-Net [14]	ICCV 2017	point-based	$8 \times 4K$ points	82.3	-	-
PointNet [28]	CVPR 2017	point-based	$8 \times 2K$ points	83.7	1.5GB	21.7ms
3D-UNet [6]	MICCAI 2016	voxel-based	8×96^3 voxels	84.6	8.8GB	682.1ms
SO-Net [18]	CVPR 2018	point-based	$8 \times 1K$ points	84.6	-	-
SCN [51]	CVPR 2018	point-based	$8 \times 1K$ points	84.6	-	-
SPLATNet [37]	CVPR 2018	point-based	-	84.6	-	-
KCNet [34]	CVPR 2018	point-based	$8 \times 2K$ points	84.7	-	-
RSNet [11]	CVPR 2018	point-based	$8 \times 2K$ points	84.9	0.8GB	74.6ms
PointNet++ [30]	NeurIPS 2017	point-based	$8 \times 2K$ points	85.1	2.0GB	77.9ms
DGCNN [47]	SIGGRAPH 2019	point-based	$8 \times 2K$ points	85.1	2.4GB	87.8ms
PCNN [3]	SIGGRAPH 2018	point-based	$8 \times 2K$ points	85.1	-	-
SpiderCNN [54]	ECCV 2018	point-based	$8 \times 2K$ points	85.3	6.5GB	170.7ms
GSNet [52]	AAAI 2020	point-based	-	85.3	-	-
3D-GCN [20]	TPAMI 2021	point-based	$8 \times 2K$ points	85.3	-	-
MVPCNN _(0.25×Ch)	-	voxel-point-based	$8 \times 2K$ points	85.5	1.7GB	19.8ms
MVPCNN _(0.5×Ch)	-	voxel-point-based	$8 \times 2K$ points	85.7	2.1GB	31.0ms
mIoU > 86.0						
PointCNN [19]	NeurIPS 2018	point-based	$8 \times 2K$ points	86.1	2.5GB	135.8ms
SPNet [21]	ECCV 2020	point-based	$8 \times 2K$ points	86.2	-	-
CF-SIS [49]	ACM MM 2020	point-based	$8 \times 2K$ points	86.2	-	-
PVCNN [23]	NeurIPS 2019	voxel-point-based	$8 \times 2K$ points	86.2	1.6GB	50.7ms
RS-CNN [22]	CVPR2019	point-based	$8 \times 2K$ points	86.2	-	-
MVPCNN _(1×Ch)	-	voxel-point-based	$8 \times 2K$ points	86.5	2.8GB	81.9ms

For the sake of convenient aggregation of voxel-based module and point-based module, the output feature channels of point-based module are consistent with the output channels of voxel-based module. Without losing generality, the output features are implemented with batch normalization [12] and ReLU activation function [9], and these point-based features are marked as $P_1 = \{P_{11}, \dots, P_{1n}\} \subseteq \mathbb{R}^{C_2}$.

When both the feature information of voxel-based and point-based module is obtained, the initializing Voxel-Point neuron will output V_1 and P_1 to the transmission Voxel-

Point neuron to strengthen the point-based and voxel-based features.

3.2. Transmission Voxel-Point Neuron

The transmission Voxel-Point neuron is used to strengthen the fusion features from the initializing Voxel-Point neuron. The enhancement of feature information is reflected in two aspects: (1) increasing the neighboring collection for the individual point-based features P_1 ; (2) increasing the independence of the neighboring voxel-based features V_1 .

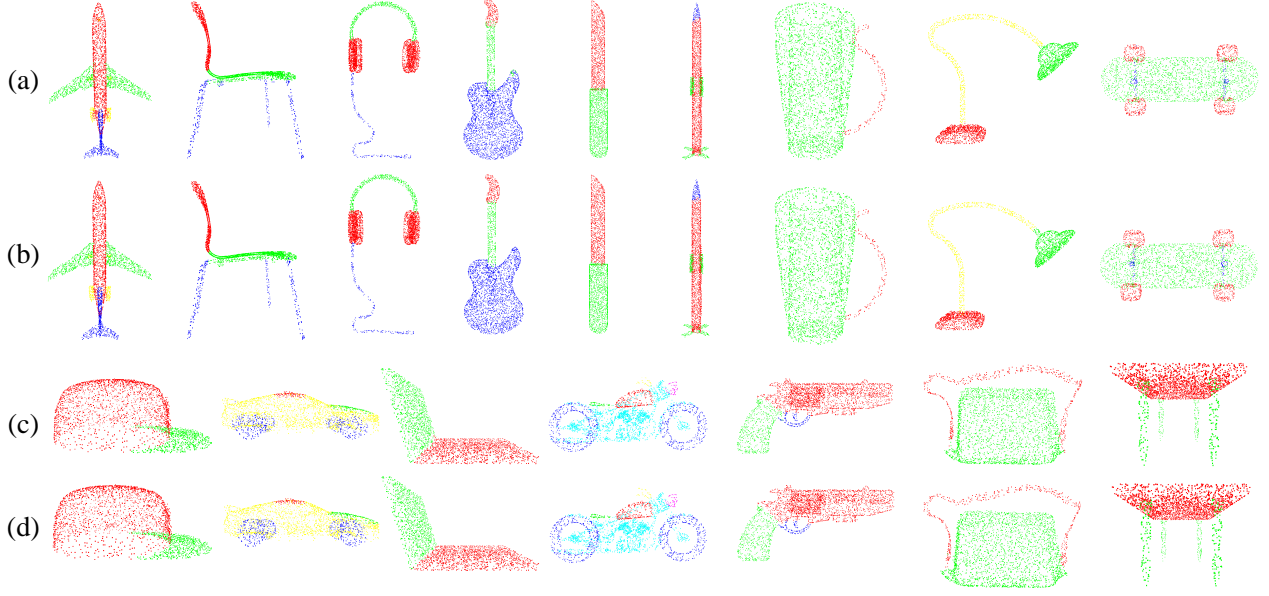


Figure 3. Segmentation results on ShapeNet Part. (a)(c) Ground truth. (b)(d) Our results.

Neighboring collection for individual point-based feature.

Transmission Voxel-Point neuron obtains the input features from the output aggregation feature information of initializing Voxel-Point neuron. In terms of network structures, the point-based module in transmission Voxel-point neuron is the same as the one in initializing Voxel-Point neuron, the voxel-based module got a little differences. The voxel-based and point-based information from the last Voxel-Point neuron have aggregated together before inputting to the next Voxel-Point neuron, but as we know, the voxel-based features V_1 have carried out information exchanging between different channels with 3D CNN, and yet the point-based features P_1 haven't exchanged. To enhance the neighboring collection for the point-based features P_1 from the last neuron with 3D CNN in the voxel-based module of the current transmission Voxel-Point neuron, we firstly fuse P_1 and V_1 to obtain the fused features $\{V_1 + P_1\} \subseteq \mathbb{R}^{C_2}$, then voxelize $\{V_1 + P_1\}$ with low spatial resolution $r \times r \times r$. In order to further strengthen the neighboring collection for P_1 and exchange the collection between different channels of V_1 , we set a 3D CNN with kernel of $1 \times 1 \times 1$ in the voxel-based module of the current transmission Voxel-Point neuron before the regular $3 \times 3 \times 3$ 3D CNN operations, thus we obtain the enhanced features $V_2 = \{V_{21}, \dots, V_{2n}\} \subseteq \mathbb{R}^{C_2}$.

Independence for the neighboring voxel-based features.

To add the independent attribute for voxel-based features V_1 , and increase the fine granularity of point-based features P_1 by the way, we adopt shared MLP to the fused features $\{V_1 + P_1\} \subseteq \mathbb{R}^{C_2}$. The parameters and network structure are consistent with the point-based module of initializing Voxel-Point neuron, and here we obtain the enhanced individual

features $P_2 = \{P_{21}, \dots, P_{2n}\} \subseteq \mathbb{R}^{C_2}$. After the completion of point-based module and voxel-based module in the transmission Voxel-Point neuron, next is to output the aggregating information. To output the final features, in addition to the transmission neuron's aggregation information, the initializing neuron's voxel-based features are also aggregated to the output, and thus we output $\{V_1 + V_2 + P_2\} \subseteq \mathbb{R}^{C_2}$ as the final features. In Section 4.5, we'll discuss the output aggregating features.

4. Experimental Results

In this section, we firstly introduce the implementation details of MVPCConv, then we compare our method with the state-of-the-art frameworks on various 3D datasets for different tasks, e.g. ShapeNet Parts (object part segmentation) [4], S3DIS (indoor scene segmentation) [2, 1] and KITTI (3D object detection) [8]. Finally, we carry on additional ablation study to certificate our proposed idea.

4.1. Implementation Details

As is shown in Figure 2, MVPCConv consists of initializing and transmission neurons, both of these two neurons including voxel-based and point-based modules, the whole framework is implemented by using Pytorch.

The initializing Voxel-Point neuron, its voxel-based modules contain two $3 \times 3 \times 3$ 3D CNNs with stride 1 and padding 1, each 3D CNN is followed by 3D batch normalization [12] and Leaky ReLU activation function [24]. The point-based SharedMLP is a 1D CNN with kernel of 1 which converts the feature channels to make it consistent

Table 2. S3DIS

Method	Reference	Type	Input Data	mIoU	mAcc	GPU Mem.	latency
mIoU < 56.0							
PointNet [28]	CVPR 2017	point-based	$8 \times 4K$ points	42.97	82.54	0.6GB	20.9ms
DGCNN [47]	SIGGRAPH 2019	point-based	$8 \times 4K$ points	47.94	83.64	2.4GB	178.1ms
3D-GCN [20]	TPAMI 2021	point-based	$8 \times 4K$ points	51.90	84.60	-	-
RSNet [11]	CVPR 2018	point-based	$8 \times 4K$ points	51.93	-	1.1GB	111.5ms
PointNet++ [30]	NeurIPS 2017	point-based	$8 \times 4K$ points	52.28	-	-	-
TanConv [40]	CVPR 2018	point-based	$8 \times 4K$ points	52.8	85.5	-	-
3D-UNet [6]	MICCAI 2016	voxel-based	8×96^3 voxels	54.93	86.12	6.8GB	574.7ms
JSNet [56]	AAAI 2020	point-based	$8 \times 4K$ points	54.5	87.7	-	-
SSNet [42]	CVPR 2020	point-based	-	55.00	61.20	-	-
MVPCNN _(0.25×Ch)	-	voxel-point-based	$8 \times 4K$ points	55.30	86.91	2.3GB	51.9ms
mIoU < 58.9							
PVCNN [23]	NeurIPS 2019	voxel-point-based	$8 \times 4K$ points	56.12	86.66	1.3GB	47.3ms
PointCNN [19]	NeurIPS 2018	point-based	$16 \times 2K$ points	57.26	85.91	4.6GB	282.3ms
Grid-GCN [53]	CVPR 2020	point-based	$8 \times 4K$ points	57.75	86.94	-	25.9ms
MVPCNN _(1×Ch)	-	voxel-point-based	$8 \times 4K$ points	58.63	87.75	4.3GB	72.7ms
mIoU > 58.9							
SPNet [21]	ECCV 2020	point-based	$8 \times 4K$ points	58.80	65.90	-	-
CF-SIS [49]	ACM MM 2020	point-based	$8 \times 4K$ points	58.90	67.30	-	-
PVCNN++ [23]	NeurIPS 2019	voxel-point-based	$4 \times 8K$ points	58.98	87.12	0.8GB	69.5ms
MVPCNN++ _(0.5×Ch)	-	voxel-point-based	$4 \times 8K$ points	60.17	88.76	2.7GB	52.6ms
MVPCNN++ _(1×Ch)	-	voxel-point-based	$4 \times 8K$ points	61.51	89.31	4.3GB	72.7ms

with the output feature channels of voxel-based module, next to the 1D CNN is 1D batch normalization [12] and ReLU activation function [9].

The transmission Voxel-Point neuron is based on the initializing voxel-point neuron, it sets the output aggregated feature of the initializing voxel-point neuron as input. Its voxel-based modules contain one $1 \times 1 \times 1$ 3D CNN with stride 1 and padding 0, and the rest part is the same as the one in the voxel-based modules of the initializing voxel-point neuron. The point-based module also keeps the output feature channels consistent with its voxel-based module.

4.2. Part Segmentation

Dataset. We extend our MVPCNN for part segmentation on ShapeNet part dataset [4]. ShapeNet part dataset including 16881 3D shapes of 16 object categories, and it is with 50 parts in all. We sample 2048 points from each shape as input training data. To be fair, we follow the typical evaluation scheme as Liu *et al.* [23], Li *et al.* [19] and Graham *et al.* [10] in our experiments.

Architecture. We use the PointNet as the backbone, and our MVPCNN is built by updating the shared MLP layers in PointNet [28] with our proposed MVPCNN layers.

Training. We set the batch size to 8, and adopt the ADAM optimizer [13] with learning rate of 0.001 for 200 epochs. The criterion is adopted with CrossEntropy. The whole training process is carried out on a single RTX 2080Ti

GPU.

Results. The mean intersection-over-union (mIoU) is utilized as evaluation metric. We adopt the same evaluation scheme in PointNet, where the IoU of each shape is calculated by averaging the same shape parts' IoUs of the 2874 test models. The mIoU is obtained by averaging the IoU of all shapes. We compare our model against the state-of-the-art point-based methods [14, 28, 18, 51, 37, 34, 11, 30, 47, 3, 54, 52, 20, 19, 21, 49, 22], voxel-based methods [6] and the newest point-voxel-based model [23]. To better balance the trade-off between time efficiency and accuracy, we also reduce the output feature channels to 50% and 25%, and marked as **MVPCNN**_(0.5×Ch) and **MVPCNN**_(0.25×Ch) respectively. Table 1 and Figure 3 presents the evaluation results of MVPCNN on the ShapeNet part dataset. Our MVPCNN outperforms the PointNet backbone significantly with 3.3% increase of mIoU, even if we reduce the latency by 8.8%, we can still obtain 2.2% mIoU ahead of PointNet. Compare with the voxel-based 3D-UNet and point-based SpiderCNN, we are **34**× faster and **8**× respectively, while achieving the better accuracy. In addition, we also outperform other point-based methods with better accuracy and higher efficiency. Notably, even compared with the voxel-point-based PVCNN, we still gain higher mIoU by 0.3% with a small amount of time efficiency lost, and PVCNN is a state-of-the-art method aimed at speed improvement.

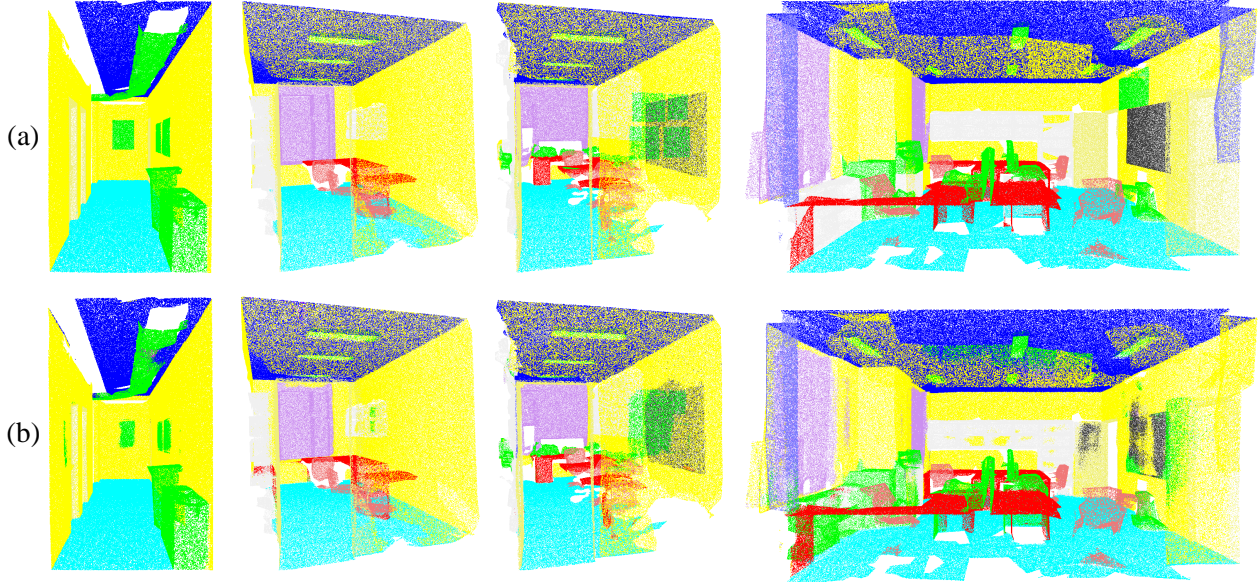


Figure 4. Segmentation results on S3DIS area5. (a) Ground truth. (b) Our results.

4.3. Indoor Scene Segmentation

Dataset. Stanford large-scale 3D Indoor Spaces (S3DIS) Dataset [2, 1] is a benchmark used for semantic indoor scene segmentation. S3DIS consists of 6 3D scanning indoor areas which totally includes 272 rooms. Similar to the operation in Liu *et al.* [23], Li *et al.* [19] and Tchampi *et al.* [41], we set Area-1, 2, 3, 4, 6 as the training set, and the rest Area-5 is used to test as it’s the only one that has no overlapping with others. We follow the data preprocessing and the evaluation criteria as Li *et al.* [19] before training, each block is sampled to 4096 points for training.

Architecture. In this task we also use PointNet as the baseline (MVPCNN), moreover, we also adopt PointNet++ as the backbone to build MVPCNN++ with MVPCNN. Similar to the experiments on ShapeNet part dataset in Section 4.2, we also design a compressed version by reducing the output feature channels to 12.5%, 25% and 50% in MVPCNN, and 50% in MVPCNN++.

Training. The batch size, optimizer, learning rate and criterion are set the same as what we have done in ShapeNet part experiments. The number of epoch is set to 50. It’s also implemented in a single RTX 2080Ti GPU.

Results. Apart from mIoU, mean accuracy (mAcc) is also used to evaluate the performance of our proposed model. In addition to comparing with the state-of-the-art point-based [28, 47, 20, 11, 30, 40, 56, 42, 19, 53, 21, 49] and voxel-based methods [6], we also compare with the newest point-voxel-based model [23]. Table 2 shows the results of all methods on S3DIS dataset, and Figure 4 presents the visualization results. Our MVPCNN improves the mIoU of the backbone (PointNet) by more than **36%**, and MVPCNN++

outperforms its backbone (PointNet++) by a large margin in mIoU of more than **17%**. Notably, The compact MVPCNN of 25% feature channel outperforms the voxel-based 3D-UNet in accuracy with more than **11** \times lower latency, and the point-based DGCNN by more than **15%** in mIoU with **3** \times lower latency. Significantly, the full model of MVPCNN outperforms the state-of-the-art point-based model (Grid-GCN and PointCNN), and we increase the speed by nearly **4** \times compared with PointCNN. At the same time, MVPCNN also outperforms the newest voxel-point-based method (PVCNN) both in mIoU and mAcc. Remarkably, the compact version of MVPCNN++ is faster than the extremely efficient voxel-point-based PVCNN++, and also outperforms it in accuracy. The full MVPCNN++ can improve the performance more than **4%** in mIoU compared with PVCNN++.

4.4. 3D Detection

Dataset. We evaluate our model on KITTI [8] for 3D detection task. This dataset is a benchmark for autonomous driving which contains 7481 training and 7518 test samples. For fair comparison, we follow the treatment of processes as Qi *et al.* [27] in our tests. Among the 7481 training samples, there are 3712 samples splitting as the *train* set, the rest 3769 is set as *val* set.

Architecture. Without changing the whole network, we set F-PointNet [27] as the backbone by replacing the shared MLP layers of the instance segmentation network with our MVPCNN to generate F-MVPCNN.

Training. The same setting for training as in part segmentation and indoor scene segmentation except that epoch is set to 209 and batch size is set to 32.

Table 3. KITTI

	Car			Pedestrian			Cyclist			Efficiency	
	Easy	Mod.	Hard	Easy	Mod.	Hard	Easy	Mod.	Hard	GPU Mem.	latency
F-PointNet [27]	85.24	71.63	63.79	66.44	56.90	50.43	77.14	56.46	52.79	1.3GB	29.1ms
F-PointNet++ [27]	84.72	71.99	64.20	68.40	60.03	52.61	75.56	56.74	53.33	2.0GB	105.2ms
F-PVCNN [23]	85.25	72.12	64.24	70.60	61.24	56.25	78.10	57.45	53.65	1.4GB	58.9ms
F-MVPCNN	85.66	72.63	64.62	71.12	62.34	57.13	79.85	58.28	54.62	2.2GB	100.0ms

Results. Mean average precision (mAP) is adopted to evaluate our model. We compare our model against F-PointNet, F-PointNet++ and F-PVCNN (whose backbone is also F-PointNet). Table 3 shows the experimental results on KITTI. Our F-MVPCNN outperforms all methods in all classes, and ours improves the mAP of F-PointNet (backbone) by up to **13.2%**. Compared with F-PointNet++, we outperform the performances of it with faster speed, especially in the hard pedestrian class.

4.5. Ablation Study

In this part, the additional ablation experiments are conducted to analyze the design idea of MVPConv. All frameworks are trained and tested on ShapeNet part datasets [4], and we consider the half of the feature channels to output as it is a good trade-off between accuracy and latency.

Effects of transmission Voxel-Point neuron for MVPConv. We have tried to enlarge the voxel resolution and directly deepen 3D CNN network of voxel-based module in initializing Voxel-Point neuron before we think about constructing the transmission Voxel-Point neuron for the whole MVPConv. As presented in the 2nd rows of Table 4, the increasing of voxel resolution could improve the performance of network in segmentation task a little bit, but the GPU memory and latency increase dramatically. Conversely, the 3rd rows of Table 4 show that the accuracy of deepening network structure by 3D convolution is reduced on the contrary, and the GPU memory and latency increased also, but the increase of them almost can be neglected. So we tried another way to deepen the network, that is the transmission Voxel-Point neuron. As shown in the 4th rows of Table 4, the transmission Voxel-Point neuron improves significant performance of MVPConv without consuming much more GPU memory and latency.

Table 4. Effects of transmission Voxel-Point neuron.

Model	mIoU	GPU Mem.	latency
Init. Neuron	85.50	1.97GB	22.3ms
Init. Neuron (1.5×R)	85.55	2.35GB	37.1ms
Init. Neuron (3×Conv3D)	85.33	2.08GB	25.1ms
Init. Neuron + Tran. Neuron	85.76	2.11GB	31.0ms

Effects of different features for MVPConv. As shown

in Table 5, we study the importance of the four feature components of MVPConv. The 1st row indicates that the performance of MVPConv is greatly degraded if only the feature of V_2 is aggregated, as the voxel-based feature V_2 is not enough for 3D learning. The feature aggregations of D, F, G and H significantly improve the performances of MVPConv, as V_2 , and the combination of $V_1 + V_2 + P_2$ achieves the best performance.

Table 5. Effects of different features for MVPConv.

Model	V_1	P_1	V_2	P_2	mIoU
A			✓		85.39
B	✓	✓			85.50
C		✓	✓		85.43
D			✓	✓	85.58
E	✓	✓	✓		85.46
F		✓	✓	✓	85.54
G	✓		✓	✓	85.76
H	✓	✓	✓	✓	85.57

Effects of $1 \times 1 \times 1$ 3D CNN for MVPConv. In Table 6, we research the effect of $1 \times 1 \times 1$ 3D CNN for MVPConv. $1 \times 1 \times 1$ 3D CNN can strengthen the information association and nonlinearity between different feature channels of point-based and voxel-based features, thus could improve the 3D learning ability of the network. As presented, almost no increase in latency and GPU memory, $1 \times 1 \times 1$ 3D CNN helps MVPConv achieve better results of accuracy.

Table 6. Effects of $1 \times 1 \times 1$ 3D CNN for MVPConv.

Model	mIoU	GPU Mem.	latency
MVPConv	85.72	2.024GB	31.2ms
MVPConv ($1 \times 1 \times 1$ CNN)	85.76	2.033GB	31.6ms

5. Conclusion

We have presented MVPConv, a 3D convolution neural network for fast and accurate 3D deep learning. Our method integrates both the voxels and points to construct initializing and transition Point-voxel neurons, which increases the

neighboring collection between point-based features and promote the independence among voxel-based features with efficient convolutions. Experimental results on multiple datasets demonstrate that our proposed method significantly improves the performances of different tasks more efficiently.

References

- [1] Iro Armeni, Sasha Sax, Amir R Zamir, and Silvio Savarese. Joint 2d-3d-semantic data for indoor scene understanding. *arXiv preprint arXiv:1702.01105*, 2017.
- [2] Iro Armeni, Ozan Sener, Amir R Zamir, Helen Jiang, Ioannis Brilakis, Martin Fischer, and Silvio Savarese. 3d semantic parsing of large-scale indoor spaces. In *CVPR*, 2016.
- [3] Matan Atzmon, Haggai Maron, and Yaron Lipman. Point convolutional neural networks by extension operators. In *SIGGRAPH*, 2018.
- [4] Angel X Chang, Thomas Funkhouser, Leonidas Guibas, Pat Hanrahan, Qixing Huang, Zimo Li, Silvio Savarese, Manolis Savva, Shuran Song, Hao Su, et al. Shapenet: An information-rich 3d model repository. *arXiv preprint arXiv:1512.03012*, 2015.
- [5] Kseniya Cherenkova, Djamila Aouada, and Gleb Gusev. Pvdeconv: Point-voxel deconvolution for autoencoding cad construction in 3d. In *ICIP*, 2020.
- [6] Özgün Çiçek, Ahmed Abdulkadir, Soeren S Lienkamp, Thomas Brox, and Olaf Ronneberger. 3d u-net: learning dense volumetric segmentation from sparse annotation. In *MICCAI*, 2016.
- [7] Dong Du, Zhiyi Zhang, Xiaoguang Han, Shuguang Cui, and Ligang Liu. Vipnet: A fast and accurate single-view volumetric reconstruction by learning sparse implicit point guidance. In *3DV*, 2020.
- [8] Andreas Geiger, Philip Lenz, Christoph Stiller, and Raquel Urtasun. Vision meets robotics: The kitti dataset. *The International Journal of Robotics Research*, 32(11):1231–1237, 2013.
- [9] Xavier Glorot, Antoine Bordes, and Yoshua Bengio. Deep sparse rectifier neural networks. In *Proceedings of the fourteenth international conference on artificial intelligence and statistics*, pages 315–323. JMLR Workshop and Conference Proceedings, 2011.
- [10] Benjamin Graham, Martin Engelcke, and Laurens Van Der Maaten. 3d semantic segmentation with submanifold sparse convolutional networks. In *CVPR*, 2018.
- [11] Qiangui Huang, Weiyue Wang, and Ulrich Neumann. Recurrent slice networks for 3d segmentation of point clouds. In *CVPR*, 2018.
- [12] Sergey Ioffe and Christian Szegedy. Batch normalization: Accelerating deep network training by reducing internal covariate shift. In *ICML*, 2015.
- [13] Diederik P Kingma and Jimmy Ba. Adam: A method for stochastic optimization. *arXiv preprint arXiv:1412.6980*, 2014.
- [14] Roman Klokov and Victor Lempitsky. Escape from cells: Deep kd-networks for the recognition of 3d point cloud models. In *ICCV*, 2017.
- [15] Shiyi Lan, Ruichi Yu, Gang Yu, and Larry S Davis. Modeling local geometric structure of 3d point clouds using geo-cnn. In *CVPR*, 2019.
- [16] Loic Landrieu and Martin Simonovsky. Large-scale point cloud semantic segmentation with superpoint graphs. In *CVPR*, 2018.
- [17] Truc Le and Ye Duan. Pointgrid: A deep network for 3d shape understanding. In *CVPR*, 2018.
- [18] Jiaxin Li, Ben M Chen, and Gim Hee Lee. So-net: Self-organizing network for point cloud analysis. In *CVPR*, pages 9397–9406, 2018.
- [19] Yangyan Li, Rui Bu, Mingchao Sun, Wei Wu, Xinhan Di, and Baoquan Chen. Pointcnn: Convolution on x-transformed points. In *NeurIPS*, 2018.
- [20] Zhi-Hao Lin, Sheng Yu Huang, and Yu-Chiang Frank Wang. Learning of 3d graph convolution networks for point cloud analysis. *TPAMI*, 2021.
- [21] Jinxian Liu, Minghui Yu, Bingbing Ni, and Ye Chen. Self-prediction for joint instance and semantic segmentation of point clouds. In *ECCV*, 2020.
- [22] Yongcheng Liu, Bin Fan, Shiming Xiang, and Chunhong Pan. Relation-shape convolutional neural network for point cloud analysis. In *CVPR*, 2019.
- [23] Zhijian Liu, Haotian Tang, Yujun Lin, and Song Han. Point-voxel cnn for efficient 3d deep learning. In *NeurIPS*, 2019.
- [24] Andrew L Maas, Awni Y Hannun, and Andrew Y Ng. Rectifier nonlinearities improve neural network acoustic models. In *ICML*, 2013.
- [25] Daniel Maturana and Sebastian Scherer. Voxnet: A 3d convolutional neural network for real-time object recognition. In *IROS*, 2015.
- [26] Hsien-Yu Meng, Lin Gao, Yu-Kun Lai, and Dinesh Manocha. Vv-net: Voxel vae net with group convolutions for point cloud segmentation. In *ICCV*, 2019.
- [27] Charles R Qi, Wei Liu, Chenxia Wu, Hao Su, and Leonidas J Guibas. Frustum pointnets for 3d object detection from rgb-d data. In *CVPR*, 2018.
- [28] Charles R Qi, Hao Su, Kaichun Mo, and Leonidas J Guibas. Pointnet: Deep learning on point sets for 3d classification and segmentation. In *CVPR*, 2017.
- [29] Charles R Qi, Hao Su, Matthias Nießner, Angela Dai, Mengyuan Yan, and Leonidas J Guibas. Volumetric and multi-view cnns for object classification on 3d data. In *CVPR*, 2016.
- [30] Charles R Qi, Li Yi, Hao Su, and Leonidas J Guibas. Pointnet++: Deep hierarchical feature learning on point sets in a metric space. In *NeurIPS*, 2017.
- [31] Joseph Redmon, Santosh Divvala, Ross Girshick, and Ali Farhadi. You only look once: Unified, real-time object detection. In *CVPR*, 2016.
- [32] Shaoqing Ren, Kaiming He, Ross Girshick, and Jian Sun. Faster r-cnn: towards real-time object detection with region proposal networks. *TPAMI*, 2016.
- [33] Gernot Riegler, Ali Osman Ulusoy, and Andreas Geiger. Octnet: Learning deep 3d representations at high resolutions. In *CVPR*, 2017.

- [34] Yiru Shen, Chen Feng, Yaoqing Yang, and Dong Tian. Mining point cloud local structures by kernel correlation and graph pooling. In *CVPR*, 2018.
- [35] Shaoshuai Shi, Chaoxu Guo, Li Jiang, Zhe Wang, Jianping Shi, Xiaogang Wang, and Hongsheng Li. Pv-rcnn: Point-voxel feature set abstraction for 3d object detection. In *CVPR*, 2020.
- [36] Shaoshuai Shi, Li Jiang, Jiajun Deng, Zhe Wang, Chaoxu Guo, Jianping Shi, Xiaogang Wang, and Hongsheng Li. Pv-rcnn++: Point-voxel feature set abstraction with local vector representation for 3d object detection. *arXiv preprint arXiv:2102.00463*, 2021.
- [37] Hang Su, Varun Jampani, Deqing Sun, Subhransu Maji, Evangelos Kalogerakis, Ming-Hsuan Yang, and Jan Kautz. Splatnet: Sparse lattice networks for point cloud processing. In *CVPR*, 2018.
- [38] Haotian Tang, Zhijian Liu, Shengyu Zhao, Yujun Lin, Ji Lin, Hanrui Wang, and Song Han. Searching efficient 3d architectures with sparse point-voxel convolution. In *ECCV*, 2020.
- [39] Maxim Tatarchenko, Alexey Dosovitskiy, and Thomas Brox. Octree generating networks: Efficient convolutional architectures for high-resolution 3d outputs. In *ICCV*, 2017.
- [40] Maxim Tatarchenko, Jaesik Park, Vladlen Koltun, and Qian-Yi Zhou. Tangent convolutions for dense prediction in 3d. In *CVPR*, 2018.
- [41] Lyne Tchapmi, Christopher Choy, Iro Armeni, JunYoung Gwak, and Silvio Savarese. Segcloud: Semantic segmentation of 3d point clouds. In *3DV*, 2017.
- [42] Ali Thabet, Humam Alwassel, and Bernard Ghanem. Self-supervised learning of local features in 3d point clouds. In *CVPR*, 2020.
- [43] Du Tran, Lubomir Bourdev, Rob Fergus, Lorenzo Torresani, and Manohar Paluri. Learning spatiotemporal features with 3d convolutional networks. In *ICCV*, 2015.
- [44] Chu Wang, Babak Samari, and Kaleem Siddiqi. Local spectral graph convolution for point set feature learning. In *ECCV*, 2018.
- [45] Lei Wang, Yuchun Huang, Yaolin Hou, Shenman Zhang, and Jie Shan. Graph attention convolution for point cloud semantic segmentation. In *CVPR*, 2019.
- [46] Peng-Shuai Wang, Yang Liu, Yu-Xiao Guo, Chun-Yu Sun, and Xin Tong. O-cnn: Octree-based convolutional neural networks for 3d shape analysis. In *SIGGRAPH*, 2017.
- [47] Yue Wang, Yongbin Sun, Ziwei Liu, Sanjay E Sarma, Michael M Bronstein, and Justin M Solomon. Dynamic graph cnn for learning on point clouds. In *SIGGRAPH*, 2019.
- [48] Zongji Wang and Feng Lu. Voxsegnet: Volumetric cnns for semantic part segmentation of 3d shapes. *TVCG*, 2019.
- [49] Xin Wen, Zhizhong Han, Geunhyuk Youk, and Yu-Shen Liu. Cf-sis: Semantic-instance segmentation of 3d point clouds by context fusion with self-attention. In *ACM MM*, 2020.
- [50] Zhirong Wu, Shuran Song, Aditya Khosla, Fisher Yu, Linguang Zhang, Xiaoou Tang, and Jianxiong Xiao. 3d shapenets: A deep representation for volumetric shapes. In *CVPR*, 2015.
- [51] Saining Xie, Sainan Liu, Zeyu Chen, and Zhuowen Tu. Attentional shapecontextnet for point cloud recognition. In *CVPR*, 2018.
- [52] Mingye Xu, Zhipeng Zhou, and Yu Qiao. Geometry sharing network for 3d point cloud classification and segmentation. In *AAAI*, 2020.
- [53] Qiangeng Xu, Xudong Sun, Cho-Ying Wu, Panqu Wang, and Ulrich Neumann. Grid-gcn for fast and scalable point cloud learning. In *CVPR*, 2020.
- [54] Yifan Xu, Tianqi Fan, Mingye Xu, Long Zeng, and Yu Qiao. Spidercnn: Deep learning on point sets with parameterized convolutional filters. In *ECCV*, 2018.
- [55] Feihu Zhang, Jin Fang, Benjamin Wah, and Philip Torr. Deep fusionnet for point cloud semantic segmentation. In *ECCV*, 2020.
- [56] Lin Zhao and Wenbing Tao. Jsnet: Joint instance and semantic segmentation of 3d point clouds. In *AAAI*, 2020.
- [57] Yin Zhou and Oncel Tuzel. Voxelnet: End-to-end learning for point cloud based 3d object detection. In *CVPR*, 2018.

Supplementary Materials

In the supplementary materials, we show more comparable visualization results in part segmentation (Figure 5, Figure 6, Figure 7 and Figure 8) and indoor scene segmentation (Figure 9, Figure 10, Figure 11, Figure 12 and Figure 13) tasks with PointNet [28], PointNet++ [30], PVCNN [23] and our MVPCNN. Besides, we will make our code and models publicly available.

1. Part Segmentation

2. Indoor Scene Segmentation

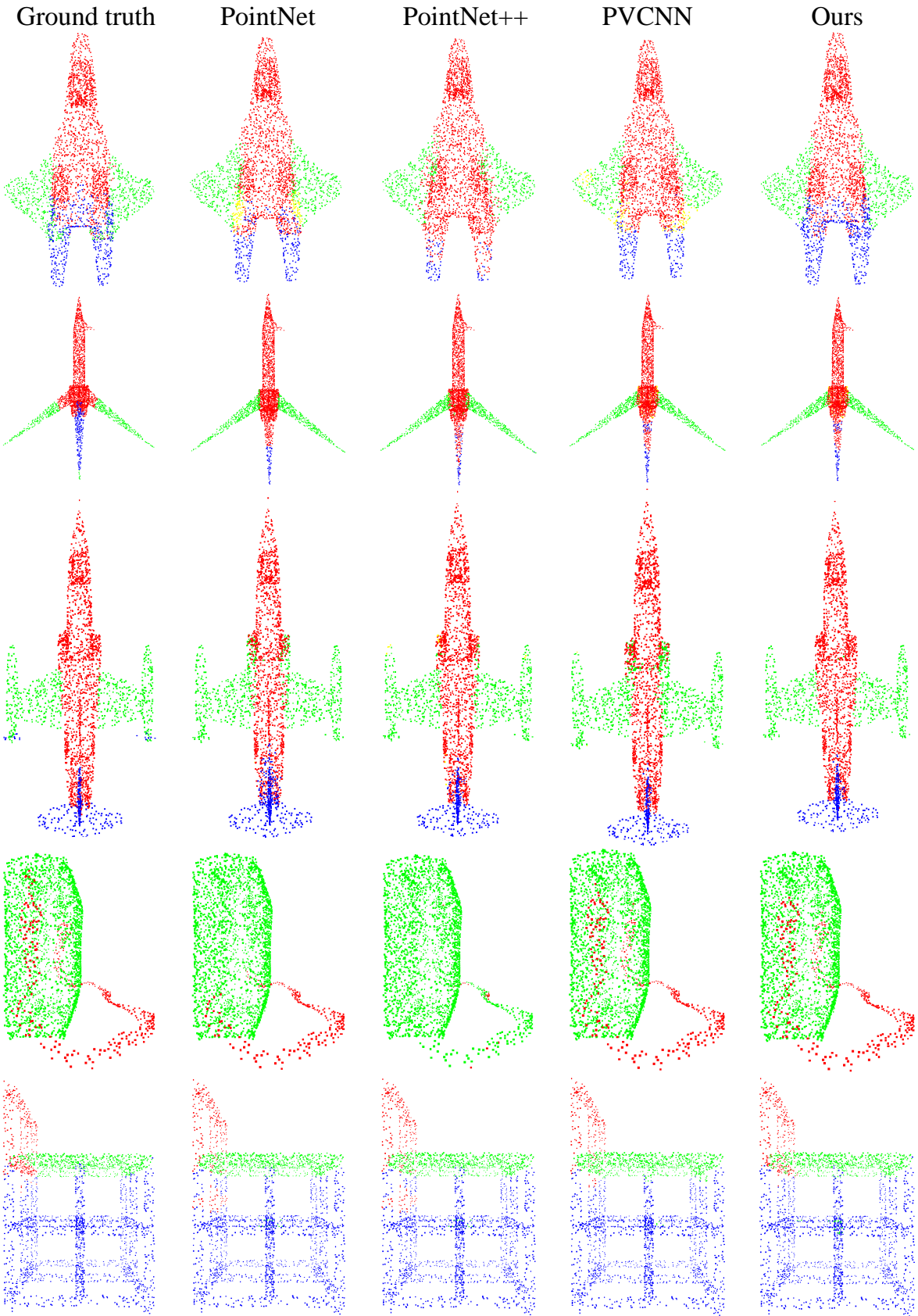


Figure 5. Part segmentation results of PointNet [28], PointNet [30] PVCNN [23] and our MVPCNN on Shapenet Part.

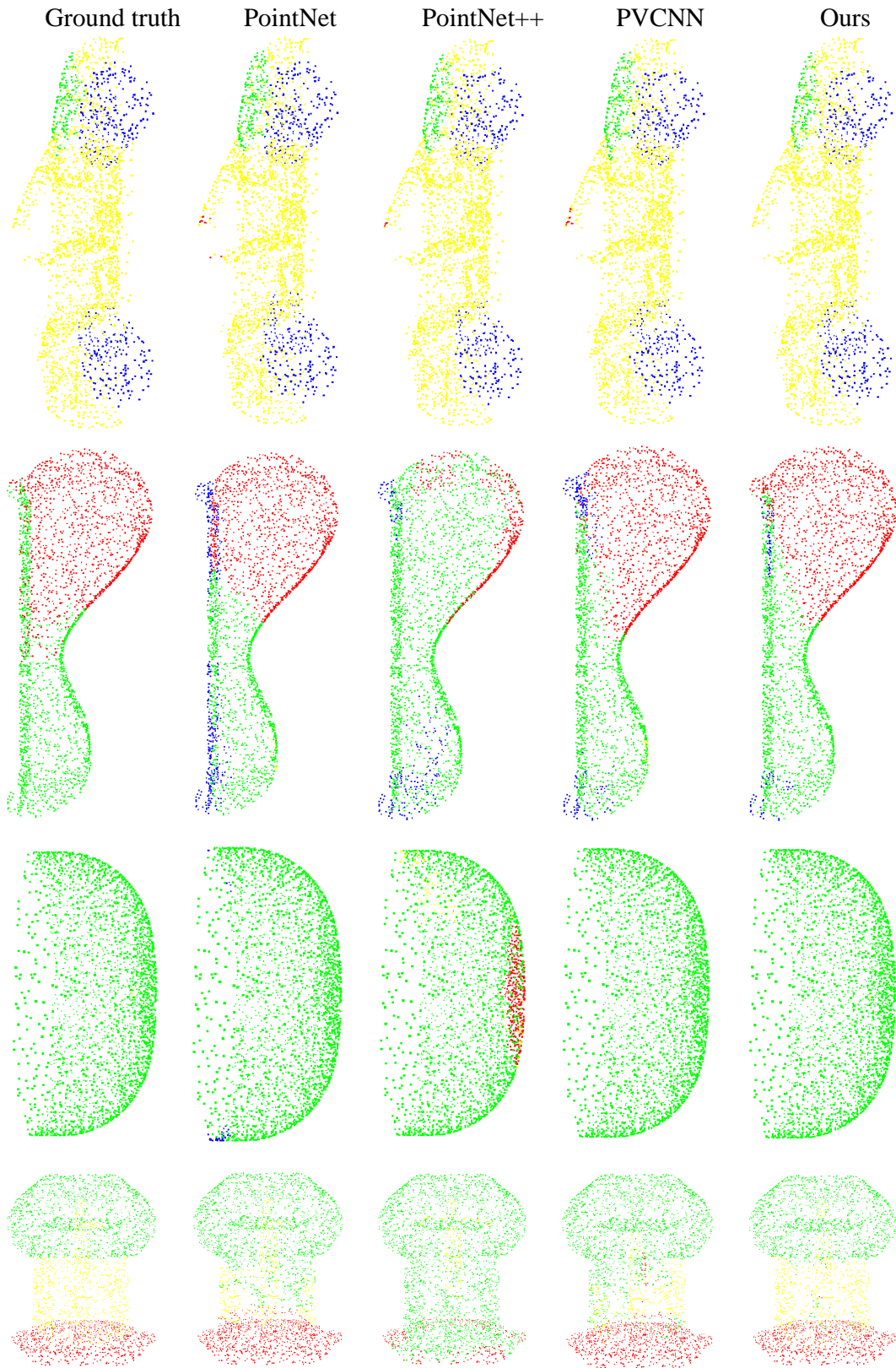


Figure 6. Part segmentation results of PointNet [28], PointNet [30] PVCNN [23] and our MVPCNN on Shapenet Part.

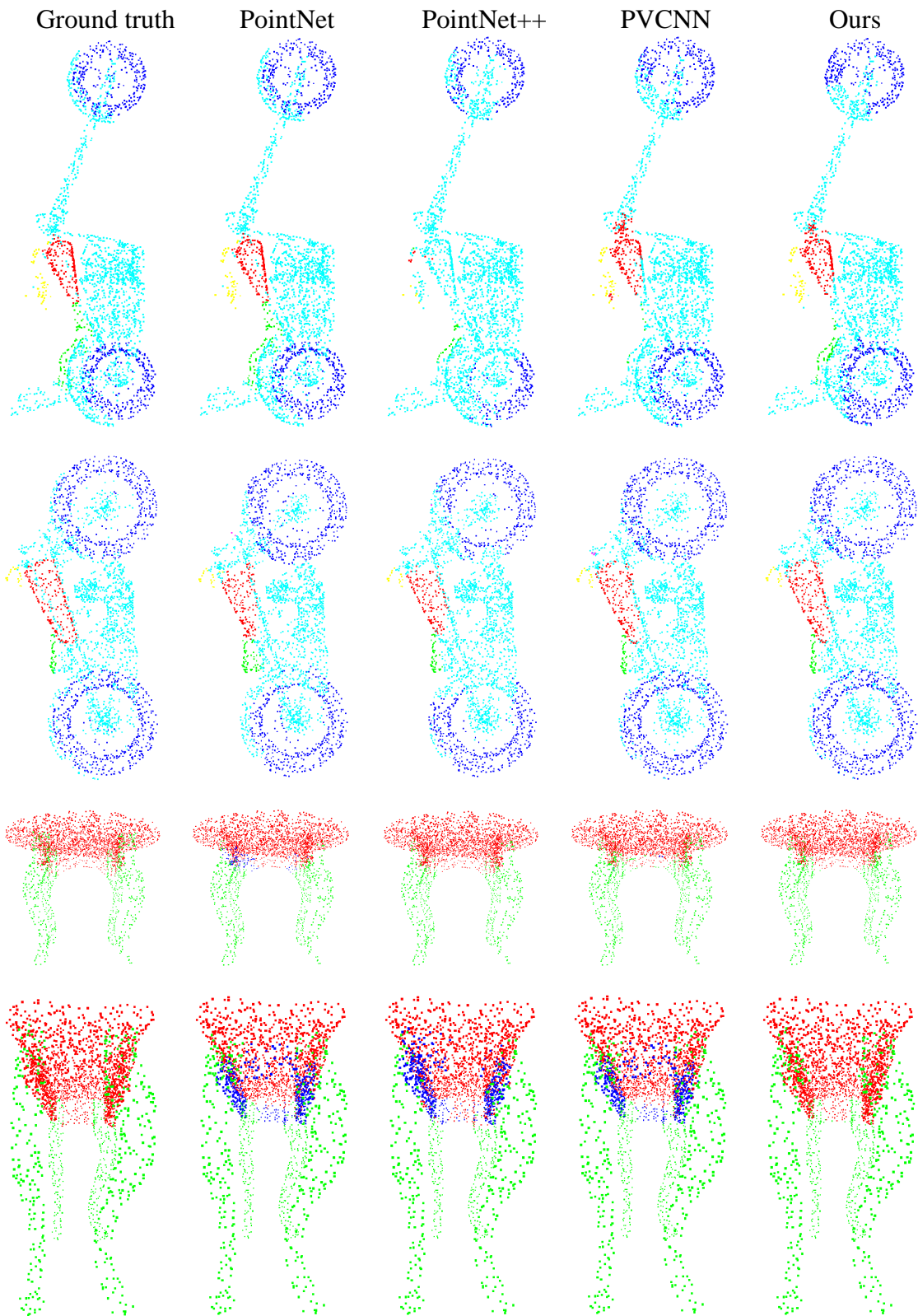


Figure 7. Part segmentation results of PointNet [28], PointNet [30] PVCNN [23] and our MVPCNN on Shapenet Part.

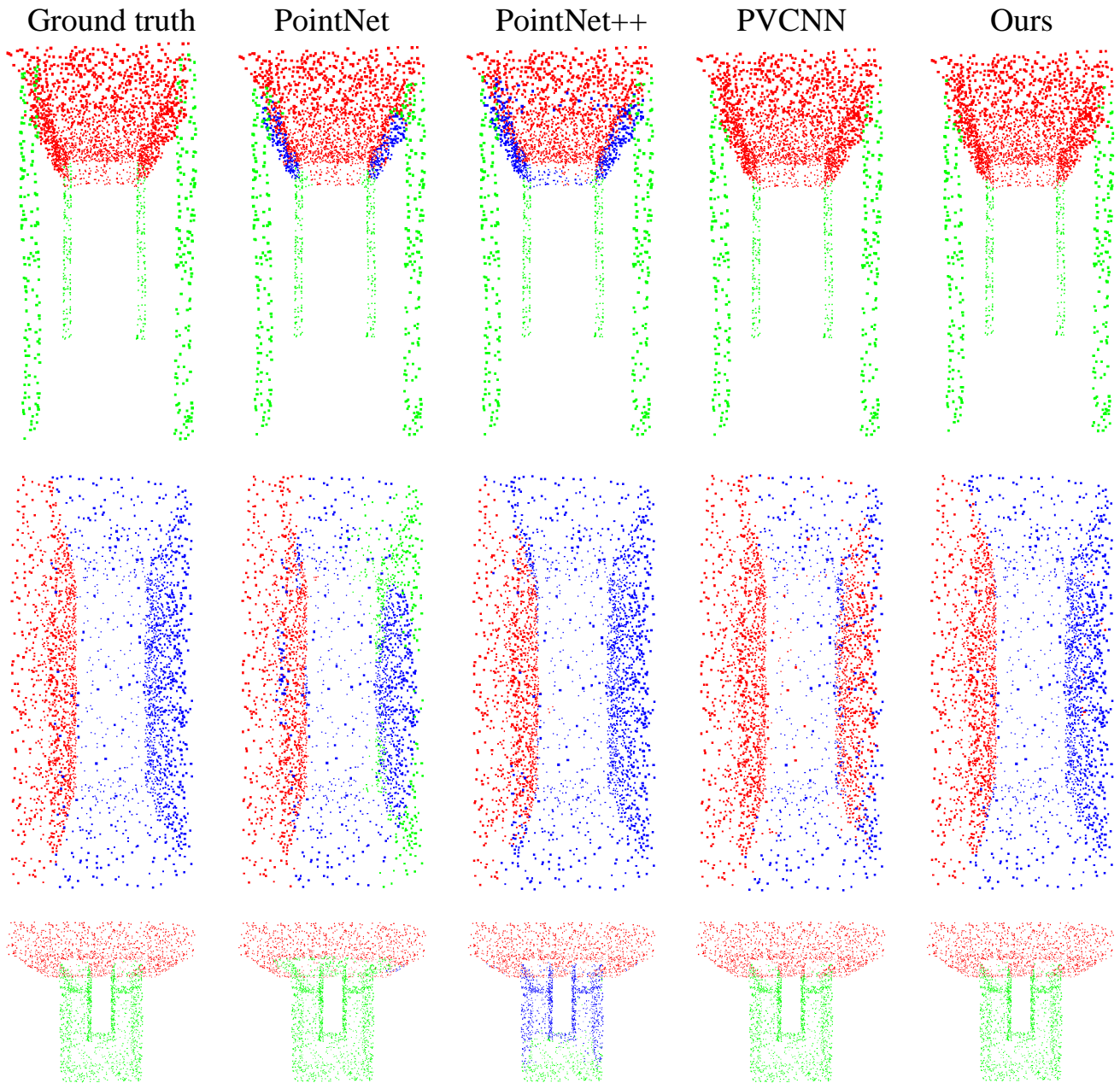


Figure 8. Part segmentation results of PointNet [28], PointNet [30] PVCNN [23] and our MVPCNN on Shapenet Part.



Figure 9. Indoor scene segmentation results of PointNet [28], PVCNN [23] and our MVPCNN on S3DIS are5.

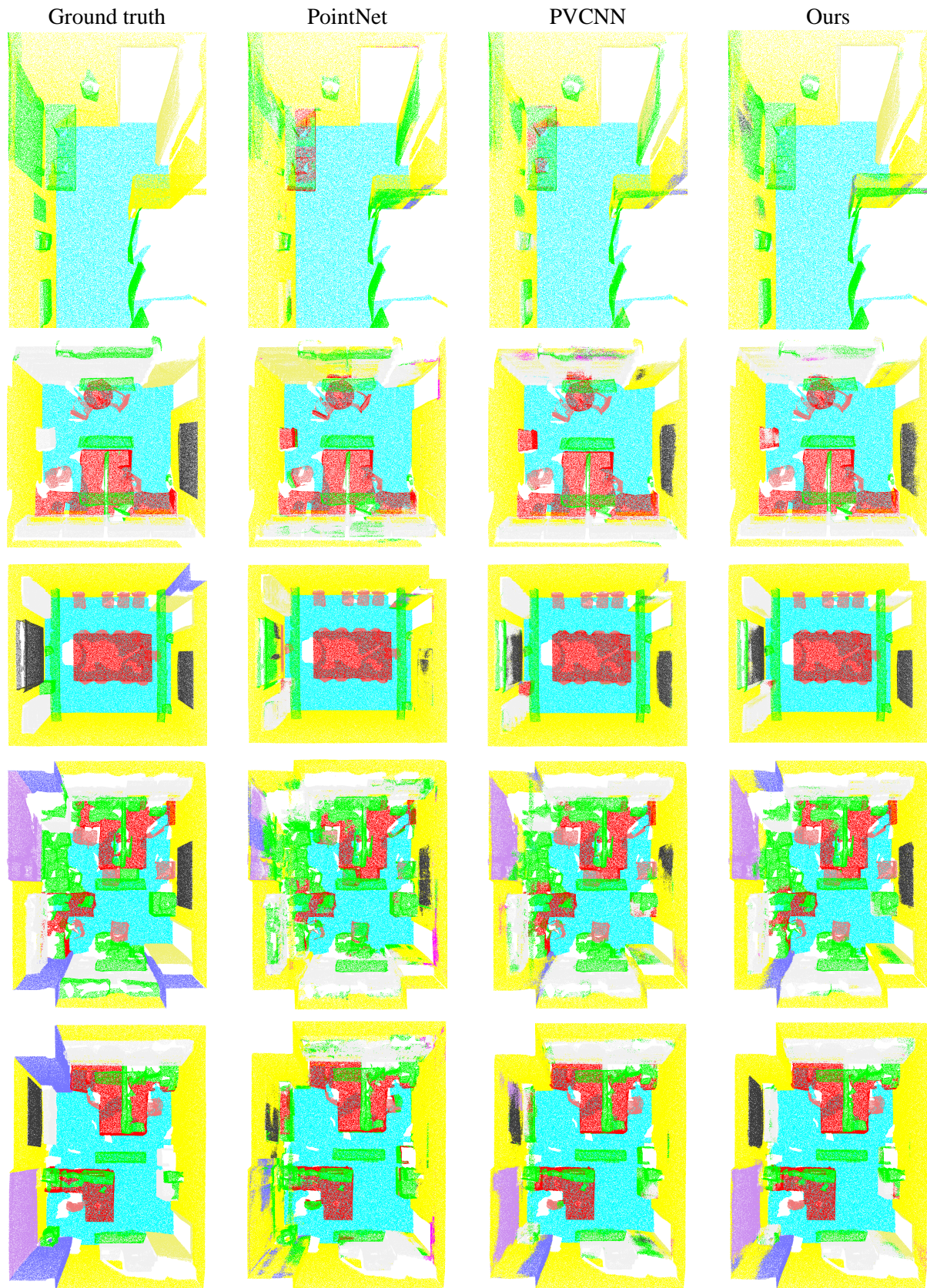


Figure 10. Indoor scene segmentation results of PointNet [28], PVCNN [23] and our MVPCNN on S3DIS are5.

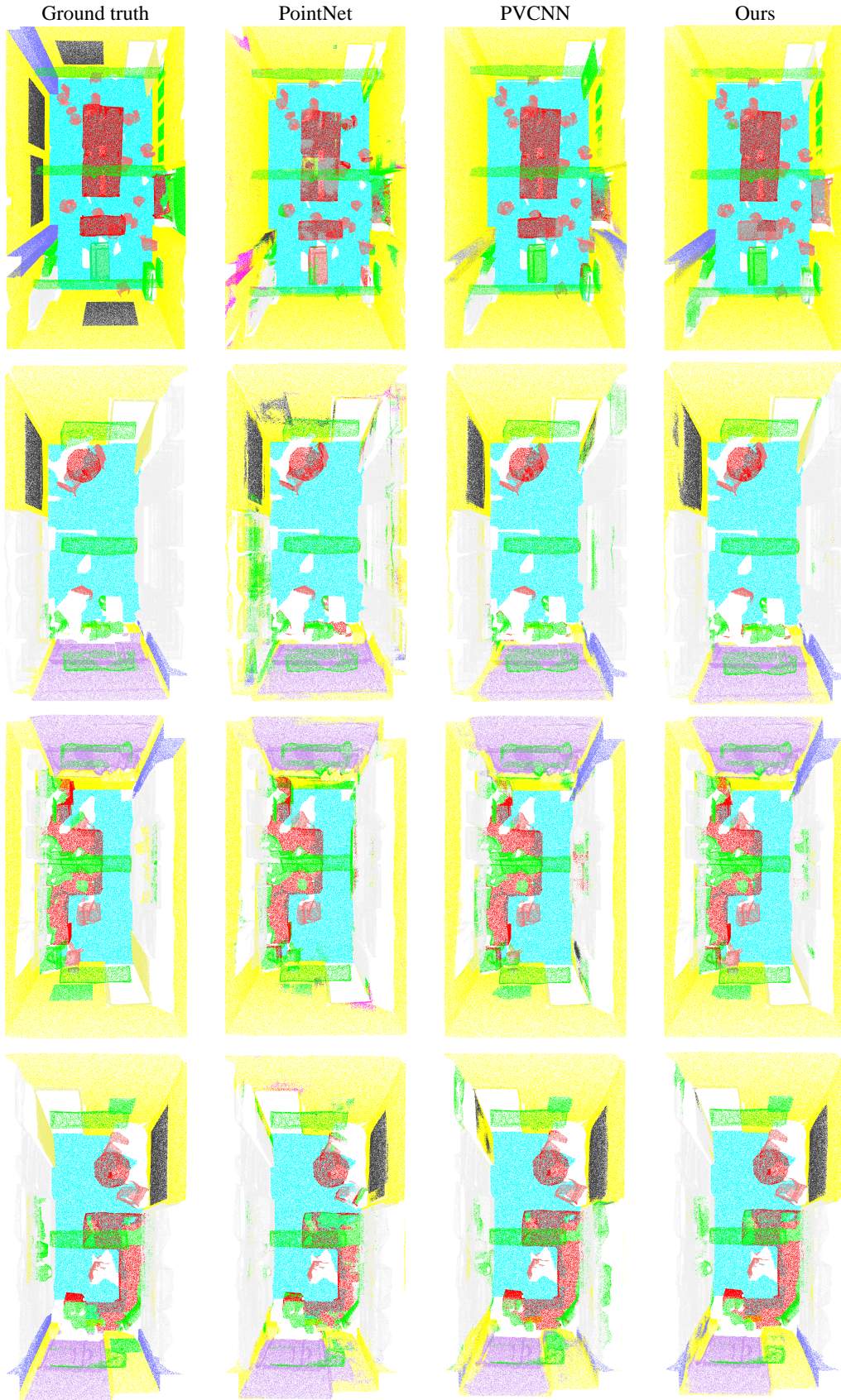


Figure 11. Indoor scene segmentation results of PointNet [28], PVCNN [23] and our MVPCNN on S3DIS are5.



Figure 12. Indoor scene segmentation results of PointNet [28], PVCNN [23] and our MVPCNN on S3DIS are5.

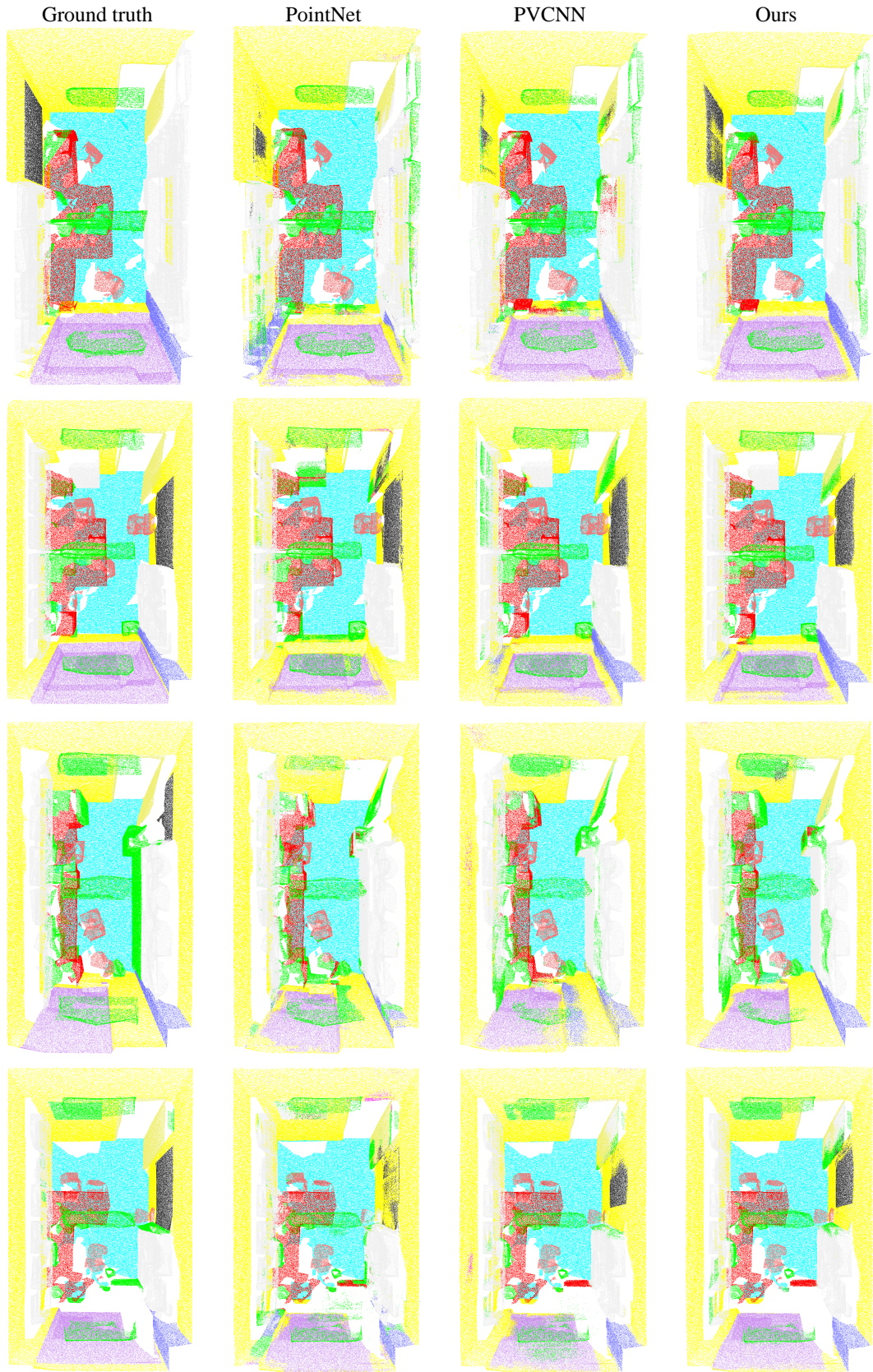


Figure 13. Indoor scene segmentation results of PointNet [28], PVCNN [23] and our MVPCNN on S3DIS are5.